The Astrophysical Journal Letters, 830:L36 (5pp), 2016 October 20 doi:10.3847/2041-8205/830/2/L36

CYGNUS X-3: ITS LITTLE FRIEND'S COUNTERPART, THE DISTANCE TO CYGNUS X-3, AND OUTFLOWS/JETS

M. L. McCollough[1], L. Corrales[2], and M. M. Dunham[1,3]
[1] Smithsonian Astrophysical Observatory, 60 Garden Street, Cambridge, MA 02138, USA; mmccollough@cfa.harvard.edu
[2] Kavli Institute for Astrophysics and Space Research, Massachusetts Institute of Technology, Cambridge, MA 02139, USA
[3] Department of Physics, State University of New York at Fredonia, Fredonia, NY 14063, USA
Received 2016 July 22; revised 2016 October 3; accepted 2016 October 4; published 2016 October 20

ABSTRACT

Chandra observations have revealed a feature within 16″ of Cygnus X-3 that varied in phase with Cygnus X-3. This feature was shown to be a Bok globule that is along the line of sight to Cygnus X-3. We report on observations made with the Submillimeter Array to search for molecular emission from this globule, also known as Cygnus X-3's "Little Friend." We have found a counterpart in both ^{12}CO (2-1) and ^{13}CO (2-1) emission. From the velocity shift of the molecular lines we are able to find two probable distances based on the Bayesian model of Milky Way kinematics of Reid et al. For the LF velocity of −47.5 km s^{-1}, we find distances of 6.1 ± 0.6 kpc (62% probability) and 7.8 ± 0.6 kpc (38% probability). This yields distances to Cyg X-3 of 7.4 ± 1.1 kpc and 10.2 ± 1.2 kpc, respectively. Based on the probabilities entailed, we take 7.4 ± 1.1 kpc as the preferred distance to Cyg X-3. We also report the discovery of bipolar molecular outflow, suggesting that there is active star formation occurring within the Little Friend.

Key words: ISM: jets and outflows – stars: formation – X-rays: binaries – X-rays: individual (Cygnus X-3) – X-rays: ISM

Supporting material: animation

1. INTRODUCTION

Cygnus X-3 is a high-mass X-ray binary (HXRB) that lies in the Galactic plane (79°.84, +0°.70). Its X-ray emission is modulated by a factor of ∼2.5 on a 4.8 hr orbital period. At an estimated distance of 9 kpc (Predehl et al. 2000), it lies behind two spiral arms of the Milky Way and the Cygnus X star-forming region, offering an opportunity to use the X-ray emission from the HXRB to probe many types of ISM structures.

Examination of *Chandra* X-ray data has shown that a small knot of X-ray surface brightness (the "Little Friend," hereafter referred to as LF; see Figure 1) located 15″.6 from the binary is modulated with the same period, but shifted in phase by 0.56 (Heindl et al. 2003; McCollough et al. 2013, hereafter referred to as MSV). The phase shift and spectrum of the feature are consistent with the phenomenon of X-ray scattering by dust in the interstellar medium (Overbeck 1965; Rolf 1983).

The angular size, spectrum, and estimated distance to the feature of 7 kpc imply that the scattering comes from a dusty 2–24 $M_\odot$ cloud (gas + dust) confined to a region that is 0.2 pc across. These are the characteristics of a Bok globule (Bok & Reilly 1947; Clemens et al. 1991). Since a Bok globule is a small molecular cloud, we might predict that it could be detected in CO emission. To see if this is possible we have observed the LF with the Submillimeter Array (SMA) and compared the resulting observations with the *Chandra* X-ray observations of the LF.

2. OBSERVATIONS

2.1. Chandra Observations

The *Chandra* observation used for this analysis was a 50 ks quenched state observation (OBSID:6601). During this quenched state the X-ray was high (*RXTE*/ASM: 2–12 keV count rates were ∼25–30 cts s^{-1}), the hard X-ray was very low (*Swift*/BAT: 15–50 keV band had an average count rate of ∼0.0 cts s^{-1}), and the radio was low (Ryle radio telescope (Pooley 2011): 15 GHz radio fluxes were ∼1 mJy). These values are all typical of a Cygnus X-3 quenched state (Waltman et al. 1996; McCollough et al. 1999; Szostek et al. 2008).

In order to understand the structure of the LF we used ZHTOOLS (Vikhlinin 2012) to create and remove the PSF of Cygnus X-3. From the right half of the zero-order image we created a radial profile (mkprof) and in turn used this to create a Cygnus X-3 PSF image (prof2img). We then subtracted and normalized the image using the PSF image (imarith). We finally mask out the readout streak to improve the dynamic range of the image. The final smoothed image (3-pixel Gaussian smooth) is shown in Figure 1. One can clearly see the LF, as well as an extended feature to the left. This type of extension is typical of what is seen in Bok globules. A movie showing the Cygnus X-3 phase dependence of the LF has been created (see Figure 1). The dark vertical feature seen on the right side is instrumental (the result of a detector node boundary).

In our analysis of these observations, we used version 4.3 of the CIAO tools. The *Chandra* data retrieved from the archive were processed with ASCDS version 7.7.6 or higher.

2.2. SMA Observations

Two tracks of observations of Cygnus X-3's LF were obtained with the SMA on 2015 September 7 and 9 in the compact configuration with seven antennas, providing projected baselines ranging from 6 to 74 m. A single pointing was observed at a phase center of R.A. = 20:32:27.1, decl. = +40:57:33.8 (J2000). The observations were obtained with the 230 GHz receiver tuned to approximately 230 GHz (1.3 mm). The correlator was configured to provide

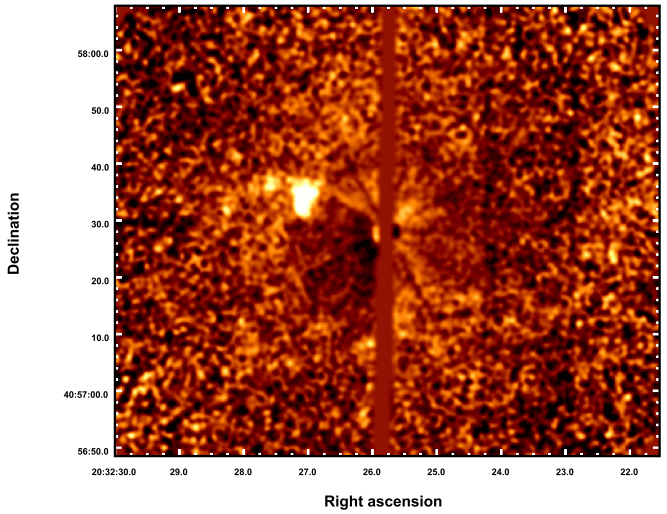

Figure 1. This is a smoothed X-ray (1–8 keV) image of the Little Friend with Cygnus X-3's PSF removed and the readout streak mask out. One can clearly see the LF and that it appears to lie along an arc with two knots of emission further out. To better visualize the phase relationship between the feature and it structure relative to Cygnus X-3 a movie was created. The method used is the same as that used in MSV, except the Cygnus X-3 PSF subtraction technique described in Section 2.1 was used for each frame of the movie. The movie goes through a full Cygnus X-3 orbital period, starting at phase 0.0.

(An animation of this figure is available.)

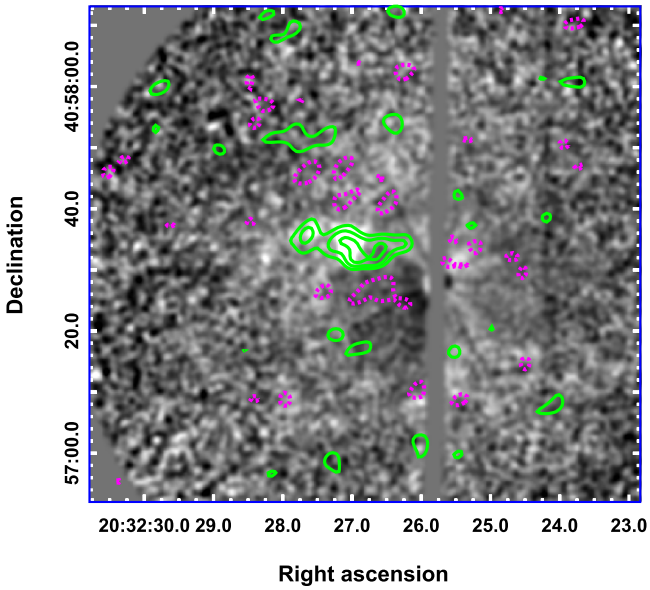

Figure 2. This is X-ray emission seen in Figure 1, for the SMA field, with contours ([−2, 2, 3, 4] × 40 mJy/beam) of ^{13}CO (2-1) at −47.5 km s^{-1} overlaid (green for positive values and dotted magenta for negative). This shows a clear association of CO emission with the LF. The CO clearly matches the X-ray emission from the LF, including the first blob to the left. Also note the extension of the ^{13}CO (2-1) to the right, away from the LF.

simultaneous observations of the ^{12}CO, ^{13}CO, and C^{18}O $J = 2$–1 lines along with the 230 GHz continuum. The observations were obtained in moderate weather conditions, with the zenith opacity at 225 GHz ranging between 0.2 and 0.3 and the system temperatures ranging between 350 and 1000 K, depending on elevation. Regular observations of the calibration sources sources mwc349a and bllac were interspersed with those of the LF for gain calibration. 3c454.3 was used for bandpass calibration, and Uranus and Neptune were used for absolute flux calibration. We conservatively estimate a 20% uncertainty in the absolute flux calibration. The data were inspected, flagged, and calibrated following standard techniques using the MIR software package.[4] They were then imaged, again following standard techniques, using the Multichannel Image Reconstruction, Image Analysis, and Display software package configured for the SMA.[5]

Combining both tracks, the continuum observations obtained a 1σ rms of 1.1 mJy beam^{-1} at a central frequency of 226 GHz, with a beam size and position angle of $3\farcs4 \times 2\farcs5$ and $-65\fdg2$, respectively. The ^{12}CO $J = 2$–1 observations obtained a 1σ rms of 51 mJy beam^{-1} in 1.0 km s^{-1} channels, with a beam size and position angle of $3\farcs3 \times 2\farcs4$ and $-64\fdg4$, respectively. The ^{13}CO $J = 2$–1 observations obtained a 1σ rms of 40 mJy beam^{-1} in 2.5 km s^{-1} channels, with a beam size and position angle of $3\farcs4 \times 2\farcs5$ and $-64\fdg4$, respectively. The C^{18}O are not discussed here.

3. COUNTERPART TO CYGNUS X-3'S LITTLE FRIEND

From the SMA observations we found the following:

Confirmation of Bok globule properties. We clearly detect the LF both in ^{12}CO (2-1) and ^{13}CO (2-1) in the velocity range between −44 and −49 km s^{-1}. Since the ^{13}CO (2-1) emission is less abundant than ^{12}CO (2-1), detectable emission is confined to the globule itself. It is thus less spatially extended than the ^{12}CO (2-1) emission and less subjected to spatial filtering in the interferometer observations, and as a result it is expected to be a better tracer of the globule structure. Indeed, it closely matches the structure seen in the X-ray. In Figure 2 we see that the strongest ^{13}CO (2-1) emission that is observed at −47.5 km s^{-1} (represented by the contours) overlays the X-ray emission from the LF.

Dust cloud properties. We did not detect any continuum thermal dust emission in our observations. The noise in the continuum at 1.3 mm was 1.1 mJy/beam in our observation. This non-detection of the dust continuum means that the LF must be at the low-mass end of what is expected for Bok Globules. Using our lower flux limit we find a 3σ mass limit of 4.2 $M_\odot$ (total gas+dust mass, so a dust mass upper limit of 0.042 $M_\odot$, assuming a standard gas-to-dust ratio). This estimate is subject to factors of two uncertainty, depending on the exact temperature and opacity of the dust grains. This constrains the Bok Globule to be on the lower end of the mass range inferred from the X-ray data.

The Distance to the Little Friend. If we assume that the velocity shift of the CO (2-1) line is primarily due to Galactic rotation, this will allow us to pinpoint the distance to the LF. Based on a study of trigonometric parallaxes of star-forming regions, Reid et al. (2009) provide a method and code that allows us to calculate the kinematic distance to the LF. Using the location of the LF (R.A. : $20^{\rm h}32^{\rm m}27\fs1$, decl. : $+40\arcdeg57\arcmin33\farcs8$) we calculate the kinematic distance as a function of velocity using the code from Reid et al. (2009) with updated solar parameters values from model A5 of Reid et al. (2014). We estimated the error in the distance by assuming systematic errors of ±7 km s^{-1} in velocity measurements ($V_{\rm LSR}$), as was done in Reid et al. (2009). We find that for a velocity of −47.5 km s^{-1} the LF has a distance of 7.62 ± 0.62 kpc.

[4] Available at https://www.cfa.harvard.edu/~cqi/mircook.html
[5] Available at http://www.cfa.harvard.edu/sma/miriad/

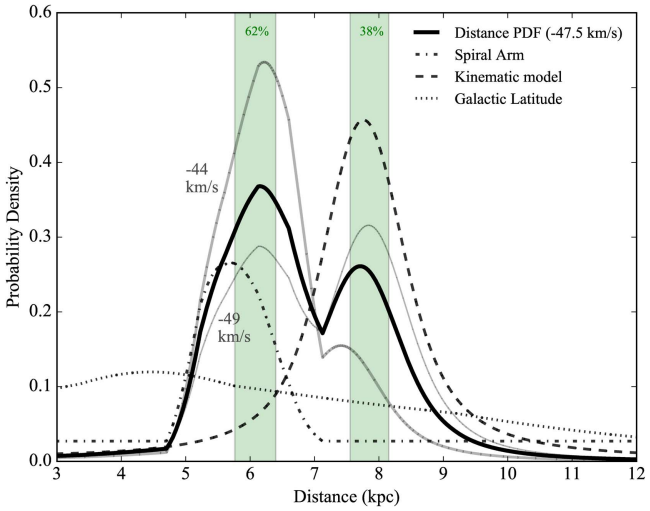

Figure 3. Probability density as a function of distance for Cygnus X-3 using a $V_{\rm LSR}$ of -47.5 km s^{-1}. The values come from the Bayesian distance estimator of Reid et al. (2016). The thick black solid line is the joint probability density. The dash–dotted, dashed, and dotted lines are the principle components in the model (spiral arm, kinematic distance, and Galactic latitude, respectively). The green shaded areas represent possible locations (with probabilities) whose widths represent $1 \pm \sigma$ uncertainties in location. The thick and thin gray lines represent the probability densities for the minimum and maximum $V_{\rm LSR}$ observed for CO emission.

But Xu et al. (2006) have noted that parts of the Perseus arm (which is in the direction of the LF) have shown anomalous motions that may lead to larger errors in the estimated kinematic distances. To address this we used a parallax-based distance estimator tool[6] (Reid et al. 2016) that uses a Bayesian approach to account for spiral arm signatures, kinematic distance estimates, Galactic latitude, and measured parallaxes to determine source distances and their associated probabilities. We ran this tool using a velocity of -47.5 km s^{-1} for the LF and arrive at a distance of 6.08 ± 0.64 kpc with a 62% probability (see Figure 3). We also find a secondary peak (38% probability) at 7.85 ± 0.6 kpc that corresponds to what we found from the kinematic distance estimate alone. It should be noted that at the largest velocity (-49 km s^{-1}) at which we detect CO emission, the probabilities for these two locations become equal.

This confirms that the LF is the most distant Bok Globule known to date. The size of the central X-ray and CO (2-1) emission of the LF is from a region of size $\sim 0.11 \times 0.16$ pc, corresponding to $(2.3 \times 3.3) \times 10^4$ au. For the distance of 6.08 kpc it is of interest to note that the LF will be located in the middle of the Perseus arm at a location where the local branch joints it (Xu et al. 2013). This is an area in which one would expect to find active star formation.

4. DISTANCE TO CYGNUS X-3

Now that we have the distance to the LF we can use the X-ray small angle scattering relationship between the LF and Cygnus X-3 (Equation (3) of MSV),

$$\Delta t = 1.15 \Theta_{\rm obs}^2 \frac{Dx}{1-x}, \quad (1)$$

to determine the distance to Cygnus X-3. From MSV we know $\Delta t = (0.56 \pm 0.02) t_{\rm cx3}$, where $t_{\rm cx3} = 17.25$ ks is the observed orbital period of Cygnus X-3, $\Theta_{\rm obs} = 15\farcs6$, and $Dx = 6.08 \pm 0.64$ (7.85 ± 0.6) kpc is the distance to the LF. We find the fractional distance of the Little Friend to be $x = 0.82 \pm 0.09$ (0.77 ± 0.07) kpc, which in turn gives us the distance to Cygnus X-3 of 7.41 ± 1.13 kpc (10.16 ± 1.21) kpc. Based on the probabilities entailed, we take 7.4 ± 1.1 kpc as the preferred distance to Cyg X-3. This value is in good agreement with the best distance estimate of 7.2 kpc determined from the X-ray dust scattering halo (Ling et al. 2009). This is one of the most precise determinations of Cygnus X-3's distance to date (currently uncertainty of 7–13 kpc from Predehl et al. 2000).

With the new preferred distance estimates to the LF and Cygnus X-3 we can reevaluate the relationship between the two (see the discussion in MSV). Taking the error in Δt as the main factor determining the uncertainty in the relative distance between Cygnus X-3 and the LF, we find that they are between 0.84 and 1.82 kpc apart. Of the previously suggested relations the chance that this a random alignment is still a reasonable possibility given that we are looking down the local arm and the LF is likely setting in the middle of the Perseus arm. This would also improve the microquasar jet-inflated bubble scenario as observed by Pakull et al. (2010) as a possibility. However the *s*upergiant bubble shell would be less of a possibility since the the LF is likely in a rich star-forming region and Cygnus X-3 is now well outside of the spiral arm.

But these new results lead to another interesting explanation of the relationship between Cygnus X-3 and the LF. The progenitor of Cygnus X-3 is expected to be a binary composed of two Wolf–Rayet stars that was created in a star-forming region such as that where the LF was found. When an X-ray binary is formed there is strong observational evidence that it experiences a natal kick from the supernova explosion (see Wong et al. 2014 and the references therein). If we take the separation to be $\sim$1 kpc and assume that the SN explosion that created Cygnus X-3 was between $(1–5) \times 10^6$ years ago (lifetime of Wolf–Rayet star) we then would get a natal kick of between 190 and 980 km s^{-1}, well within the range that has been observed for other X-ray binaries and pulsars (Wong et al. 2014). Hanson et al. (2000) constrained the magnitude of systemic radial velocity of Cygnus X-3 to be <200 km s^{-1}, indicating a lower value of natal kick and hence a longer time since the SN more probable. In contrast, Paerels et al. (2000) find clear indications of an $\sim$800 km s^{-1} redshift of Cygnus X-3's X-ray line spectra ,which is consistent with the upper bound of the estimated natal kick. Thus the relationship between Cygnus X-3 and the LF and their separation can be explained in terms of the natal kick at the time of the formation of Cygnus X-3 as an X-ray binary. This also explains why Cygnus X-3 does not appear to currently be in an area of rich star formation.

5. CYGNUS X-3 LITTLE FRIEND'S OUTFLOWS/JETS

A somewhat unexpected result of these observations is clear evidence of outflows/jets from the LF in both ^{12}CO (2-1) and ^{13}CO (2-1) (see Figures 2, 4, and 5). Such outflows/jets are know to occur in molecular clouds (Arce et al. 2007; Frank et al. 2014). This clearly indicates that a protostar has formed in the LF and that a molecular outflow has started to occur.

[6] Available at http://bessel.vlbi-astrometry.org/bayesian

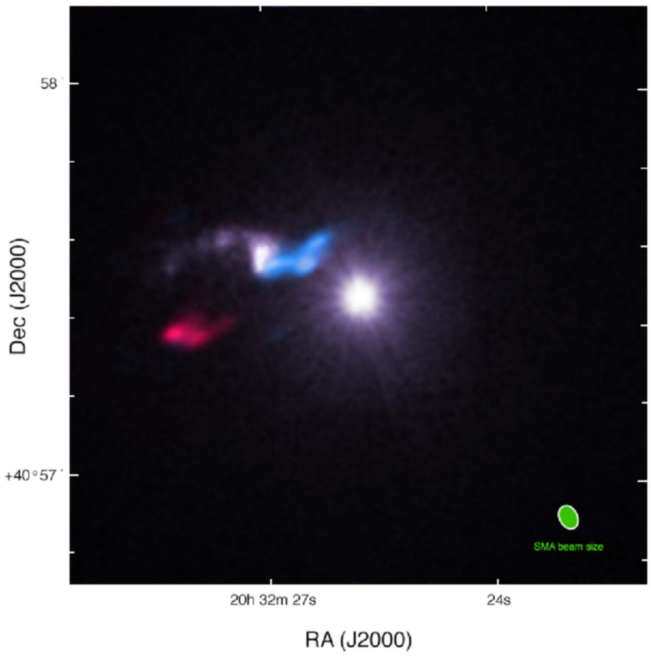

Figure 4. This is a composite image created from the X-ray (1–8 keV) *Chandra* data (purple/white) and CO emission obtained from the SMA showing the outflow/jet from the LF. In the X-ray you can see Cygnus X-3 and the LF. The blue is ^{12}CO (2-1) emission with negative velocities (0 to -2 km s^{-1}) relative to the strongest ^{13}CO (2-1), which we believe represents the rest velocity of the globule. The red is ^{12}CO (2-1) emission from positive velocities (1 km s^{-1}) that we believe are associated with the outflow/jet.

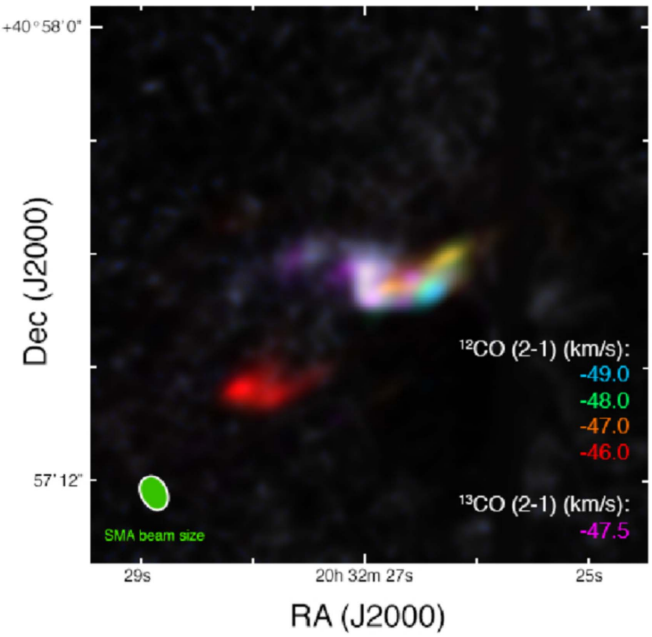

Figure 5. Cygnus X-3 PSF subtracted image (purple/white) of the LF and the CO emission. The magenta is ^{13}CO (2-1), which covers the LF as well as part of the jet. The other colors represent the various velocity components of emission from ^{12}CO (2-1) showing the velocity structure of the jets, which is discussed in the text.

In Figure 4 we can see prominent blue and redshifted outflows/jets coming from the LF. The blueshifted component (relative velocity range of 0 to -2 km s^{-1}) extends out 14″ (~0.41 pc) with an axial ratio of ~2.5. The redshifted component (relative velocity of -1 km s^{-1}) extends out 18″ (~0.53 pc), with an axial ratio of ~2.3. The blueshifted component also shows a bend in the outflow/jet at about 7″ (~0.21 pc) from the LF and make a ~40° change in the flow. The highest observed velocity (-2 km s^{-1}) flow appears as two knots, with one located at the LF and the other at the bend in the outflow/jet. The knots may indicate the location of where a shock is occurring in the outflow. From Figure 2 the ^{13}CO (2-1) emission extends from the LF to the point at which the outflow bends. The redshifted component (1 km s^{-1}) shows evidence of possible knots near its end. Similar low-velocity bipolar molecular outflows have been observed in other low-mass star-forming clouds (Dunham et al. 2011). Figure 5 shows the velocity structure of the outflow/jet. The structure that is observed may be the result of precession of the protostar or an interaction with the ISM. What this indicates is that we are seeing a jet + outflow (wind) from a newly emerging protostar with the possibility of shocks occurring.

Outflows as signposts of star formation are very commonly detected. In order to compare the outflow driven by the LF, located at a distance of 6.08 kpc, with those driven by typical low-mass protostars in nearby ($d < 500$ pc) Gould Belt clouds, we use the ^{12}CO data to calculate the mass of the LF outflow. We assume optically thin, LTE emission at an excitation temperature of 50 K (Dunham et al. 2014), and follow the procedures outlined in Dunham et al. (2014; see their Appendix C) to convert from brightness temperature to total outflow mass. The resulting outflow mass is 0.07 $M_{\odot}$.[7] Comparing to recent surveys of outflows driven by low-mass protostars in the nearby ($d < 500$ pc) Gould Belt clouds (e.g., Curtis et al. 2010; Dunham et al. 2014), the LF outflow is within but near the top end of the range of measured outflow masses (10^{-3} to a few tenths of a $M_{\odot}$). Thus this detection, at 6.08 kpc, is consistent with an outflow driven by a low-mass protostar, and suggests an outflow near the top end of the mass scale for these types of regions.

6. SUMMARY

In this study we have found the molecular counterpart to the first, and to date the most distant, Bok globule to have been seen in the X-ray. Also as a result of this work we have determined the most accurate distance to Cygnus X-3 to date (~15%). Also, as a result of this analysis we provide insight into where Cygnus X-3 likely formed and provide an estimate of a natal kick it received when the X-ray binary was formed via an SN explosion. In Figure 4 we see what can best be described as a stellar cycle of life. We have, in the X-ray from Cygnus X-3, an X-ray binary with a compact object representing an endpoint of stellar evolution. Also in the X-ray from the scattered X-rays of Cygnus X-3 we see a Bok globule (the LF), a small dense molecular cloud, from which stars are know to form. Finally, in CO emission we see outflows/jets from the LF that give a clear indication that a protostar has indeed formed and is creating an outflow.

M.L.M. wishes to acknowledge support from NASA under contract NAS8-03060. This research has made use of data obtained from the *Chandra* Data Archive and software provided by the *Chandra* X-ray Center (CXC). M.M.D. acknowledges support from the Submillimeter Array (SMA) through an SMA postdoctoral fellowship, and from NASA

[7] For the secondary distance peak the outflow would correspond to 0.11 $M_{\odot}$.

through grant NNX13AE54G. Support for the work by L.R.C. came in part from the NASA Earth and Space Science Fellowship Program, grant NNX11AO09H. This work is based primarily on observations obtained with the Submillimeter Array, a joint project between the Smithsonian Astrophysical Observatory and the Academia Sinica Institute of Astronomy and Astrophysics and funded by the Smithsonian Institution and the Academia Sinica. Special thanks go to J. DePasquale for the help with the composite X-ray and CO images. We wish to thank the referee for pointing out several important papers that helped to improve this work.

REFERENCES

Arce, H. G., Shepherd, D., Gueth, F., et al. 2007, in Protostars and Planets V, ed. B. Reipurth, D. Jewitt, & K. Keil (Tucson, AZ: Univ. Arizona Press), 245
Bok, B. J., & Reilly, E. F. 1947, ApJ, 105, 255
Brand, J., & Blitz, L. 1993, A&A, 275, 67
Clemens, D. P., Yun, J. L., & Heyer, M. H. 1991, ApJS, 75, 877
Curtis, E. I., Richer, J. S., Swift, J. J., & Williams, J. P. 2010, MNRAS, 408, 1516
Dunham, M. M., Arce, H. G., Mardones, D., et al. 2014, ApJ, 783, 29
Dunham, M. M., Chen, X., Arce, H. G., et al. 2011, ApJ, 742, 1
Frank, A., Ray, T. P., Cabrit, S., et al. 2014, in Protostars and Planets VI, ed. H. Beuther et al. (Tucson, AZ: Univ. Arizona Press), 451
Hanson, M. M., Still, M. D., & Fender, R. P. 2000, ApJ, 541, 308
Heindl, W. A., Tomsick, J. A., Wijnands, R., & Smith, D. M. 2003, ApJL, 588, L97
Ling, Z., Zhang, S., & Tang, S. 2009, ApJ, 695, 1111
Mathis, J. S., & Lee, C.-W. S. 1991, ApJ, 376, 490
McCollough, M. L., Robinson, C. R., Zhang, S. N., et al. 1999, ApJ, 517, 951
McCollough, M. L., Smith, R. K., & Valencic, L. A. 2013, ApJ, 762, 2 (MSV)
Overbeck, J. W. 1965, ApJ, 141, 864
Paerels, F., Cottam, J., Sako, M., et al. 2000, ApJL, 533, L135
Pakull, M. W., Soria, R., & Motch, C. 2010, Natur, 466, 209
Pooley, G. G. 2011, Monitoring of variable sources, X-ray binaries and AGN, at 15 GHz, http://www.mrao.cam.ac.uk/~guy/
Predehl, P., Burwitz, V., Paerels, F., & Trümpler, J. 2000, A&A, 357, L25
Reid, M. J., Dame, T. M., Menten, K. M., & Brunthaler, A. 2016, ApJ, 823, 77
Reid, M. J., Menten, K. M., Brunthaler, A., et al. 2014, ApJ, 783, 130
Reid, M. J., Menten, K. M., Zheng, X. W., et al. 2009, ApJ, 700, 137
Rolf, D. P. 1983, Natur, 302, 46
Szostek, A., Zdziarski, A. A., & McCollough, M. L. 2008, MNRAS, 388, 1001
Vikhlinin, A. 2012, ZHTOOLS: X-ray data analysis, http://hea-www.harvard.edu/RD/zhtools/
Waltman, E. B., Foster, R. S., Pooley, G. G., Fender, R. P., & Ghigo, F. D. 1996, AJ, 112, 2690
Wong, T.-W., Valsecchi, F., Ansari, A., et al. 2014, ApJ, 790, 119
Xu, Y., Li, J. J., Reid, M. J., et al. 2013, ApJ, 769, 15
Xu, Y., Reid, M. J., Zheng, X. W., et al. 2006, Sci, 311, 54